Catalysis Today 146 (2009) 196–201

Contents lists available at ScienceDirect

Catalysis Today

journal homepage: www.elsevier.com/locate/cattod

Preparation of iridium catalyst and its catalytic activity over hydrazine hydrate decomposition for hydrogen production and storage

Young Bae Jang, Tak Hee Kim, Min Ho Sun, Jun Lee, Sung June Cho *

Center for Functional Nano Fine Chemicals, Research Institute of Catalysis and Department of Applied Chemical Engineering, Chonnam National University, Gwangju 500-757, South Korea

ARTICLE INFO

Article history:
Available online 23 February 2009

Keywords:
Nanoparticle
Ir catalyst
Atomic structure

ABSTRACT

Two nanometer sized Ir nanoparticle supported on γ-Al_2O_3 both in granule and honeycomb catalyst was prepared by the repeated soak-dry processes, drying, and subsequent reduction. Highly dispersed nanoparticles spread over the catalyst surface, referred from the results of TEM, AFM, XAFS and hydrogen chemisorption. The structure of nanoparticle changed with the increase of metal content. At 5.8 wt% loading, the nanoparticle was close contact with the catalyst surface and seemed to spread like raft. Upon increasing the iridium loading to 16.4 wt%, the particle grew to spherical shape having the reduced Ir core covered with oxygen. The hydrazine hydrate decomposition proceeded readily on the honeycomb catalyst containing 2 wt% Ir when the product water in the catalyst bed was removed properly.

1. Introduction

Hydrazine, N_2H_4, as monopropellant was investigated for use in satellite propulsion using an Ir based catalyst [1]. Shell405™ (30 wt% Ir/Al_2O_3) was milestone in the development of such a catalyst, which activated anhydrous hydrazine even at 293 K. Hydrazine can be converted in the following two ways: $N_2H_4(g) \rightarrow N_2(g) + 2H_2(g)$, $\Delta H = -95.4$ kJ mol^{-1} and $3N_2H_4(g) \rightarrow 4NH_3 + N_2(g)$, $\Delta H = -157$ kJ mol^{-1} [2].

The structural property of the Ir catalyst was studied extensively due to the importance of the unique catalytic activity for NH_3 and N_2H_4 decomposition for the hydrogen generation free of CO_x [3,4]. The Ir nanoparticle was prepared on zeolite and γ-Al_2O_3 support using ion exchange, incipient wetness, chemical vapor deposition, etc. The atomic structure of such nanoparticle in the supercage of the NaY zeolite and on the γ-Al_2O_3 was confirmed by XAFS [5–7]. The small Ir_4 cluster was derived when the $Ir_4(CO)_{12}$ complex was decarbonylated on the support. However, the Ir content was near 1.0 wt%. More or less higher metal content led to the formation of 1 nm sized nanoparticle consisting of 40–60 atoms in the supercage of the NaY zeolite, which was also supported by the result of EXAFS data analysis and xenon adsorption measurement [8].

Recently, we reported the preparation of 30 wt% Ir catalyst supported on γ-Al_2O_3 using dry-soak method similar to the multiple impregnation [4]. The results from the X-ray diffraction, transmission electron microscopy, hydrogen chemisorption and X-ray absorption fine structure analysis suggested the formation of Ir nanoparticle covered with oxygen. The particle size was limited to less than 2 nm though the loading was extremely high near 30 wt%.

In this work, the Ir catalyst in honeycomb type was prepared to have lower metal content using dry-soak method since the lower metal content is preferred for the commercial catalytic application such as hydrogen generation. The atomic and textural properties of Ir catalyst were probed with transmission electron microscopy, atomic force microscopy and X-ray absorption fine structure. Also, the catalytic reaction system for hydrazine hydrate decomposition was designed to investigate the catalytic property of the honeycomb containing 2 wt% Ir.

2. Experimental

2.1. Preparation of iridium catalyst

$IrCl_3$ (54.3%, Johnson Matthey) was dissolved in 80 ml of water at room temperature and aged for 48 h. A desired amount of the reinforced catalyst support (Alcoa Co.) was added to the solution and stirred for 20 min. The wet catalyst support was dried with hot air for 5 min and heated at 653 K for 15 min to remove the acidic fumes. This wetting procedure was repeated to obtain the desired iridium content. After six repetition procedures, the sample was dried at 573 K for 1 h with flowing nitrogen and subsequently reduced with a hydrogen and nitrogen mixture (10:1) at 573 K for 30 min. This intermittent drying and reduction was essential to remove the acid accumulated on the catalyst. After the final impregnation, the sample was reduced with hydrogen at 823 K for

* Corresponding author. Tel.: +82 62 530 1902.
E-mail address: sjcho@chonnam.ac.kr (S.J. Cho).

0920-5861/$ – see front matter © 2009 Elsevier B.V. All rights reserved.
doi:10.1016/j.cattod.2009.01.040

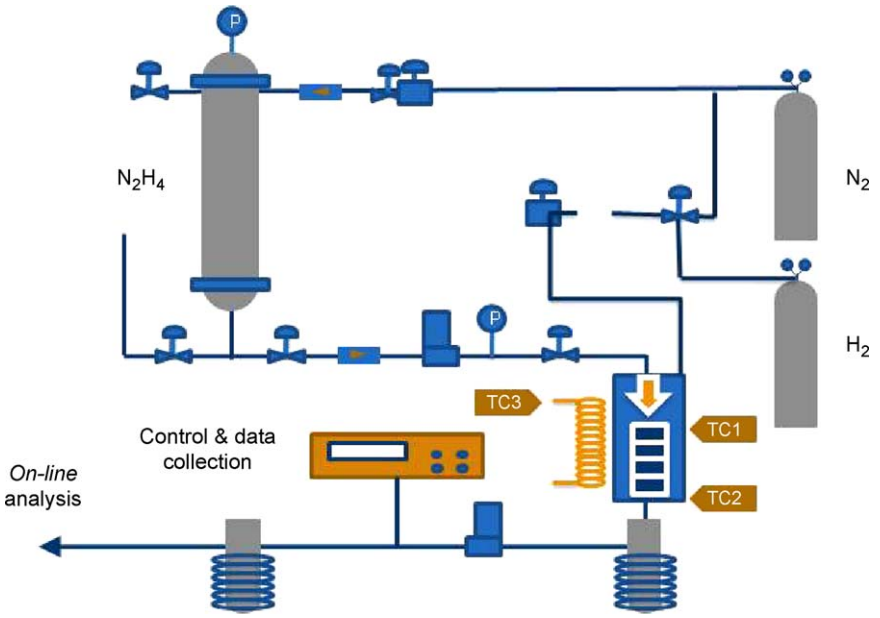

Fig. 1. Catalytic reaction system for hydrazine hydrate decomposition.

2 h. The nominal metal loading was controlled to 5, 10 and 20 wt%, respectively.

For the preparation of honeycomb catalyst, the honeycomb (DongSuh Ceracomb) of 200 cpi was wash-coated repeatedly with alumina sol containing 20 wt% boehmite (Sasol) to achieve 10 wt% alumina coating after the activation of the catalyst at 773 K. An aqueous solution of $IrCl_3$ (54.3 wt%, Johnson Matthey) was prepared using the repeated soak-dry processes similar to the preparation method for the powder form. The honeycomb containing the Ir precursor was dried in air at 773 K. It was reduced with flowing hydrogen at 573 K. The obtained catalyst contained 2 wt% Ir with respect to total weight which was equivalent to 21.2 wt% Ir content to the wash-coat alumina only.

2.2. Characterization of the iridium catalyst

Hydrogen adsorption measurements were carried out at 298 K with a conventional volumetric gas adsorption apparatus according to the method described elsewhere [9]. The phase purity and the crystallinity of the sample was determined using powder X-ray diffraction (XRD, D/MAX Ultima III, Rikagu, Japan) with Cu Kα radiation. The BET N_2 adsorption–desorption isotherms were measured at 77 K with ASAP2020 (Micromeritics, USA).

Elemental analysis was performed using an X-ray photoelectron spectroscopy (MultiLab 2000 VG, England). The field emission transmission electron micrographs were taken using Tecnai F20 (Philips) with an accelerating voltage of 200 kV. The textural image of the catalyst was obtained using AFM equipped with the 5 μm scanner (Veeco CP-II SPM).

X-ray absorption fine structure (XAFS) of the iridium catalyst was obtained under ambient conditions using R-XAS instrument (Rigaku, Japan) operating at 20 kV and 15 mA with a W filament, and also at Beamline 3C1 in the Pohang Accelerator Laboratory, Korea. The data was analyzed by the standard method using the *ab-initio* Feff program [10].

2.3. Catalytic reaction over honeycomb catalyst

The content of hydrazine in the hydrate (Daejung) was analyzed using GC. The content was 55.1 wt% corresponding to 6.8 Hwt% in terms of hydrogen storage content. The reaction system for honeycomb catalyst as shown in Fig. 1 was built in pulse injection mode where the injection time can be varied 100–500 ms depending on the reaction condition. The catalyst consisted for three honeycombs of 50 mm diameter. The volume of the product gas was monitored using the wet gasmeter. Also, the product was analyzed *on-line* with Eco Physics CLS 844 CM hr.

3. Results and discussion

Fig. 2 shows the XRD patterns of the Ir catalyst as function of metal loading. The XRD pattern showed only three major peaks at 40.5°, 46.8° and 68.7° 2θ. These peak positions were assigned to Ir metal phase, which belongs to the *fm*3*m* space group with a = 0.384 nm. In the case of 30 wt% Ir catalyst, the particle size was estimated from the Scherrer equation assuming an instrumental line broadening factor of 0.115°, which ranged from 1.5 to 1.8 nm [11]. However, the line broadening was complicated with the appearance of Al_2O_3 peaks at 46.2° and 67.6° and one broad peak around 30–40°, with decreasing metal content, making difficult to make the particle size. Still the large full width at half maximum (FWHM) suggested the formation of small Ir nanoparticles.

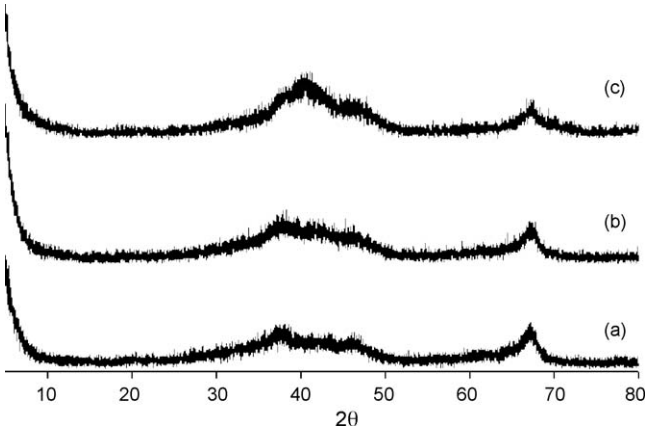

Fig. 2. X-ray diffraction patterns of the catalyst: (a) 5 wt% Ir/Al_2O_3, (b) 10 wt% Ir/Al_2O_3 and (c) 20 wt% Ir/Al_2O_3.

Table 1
Surface properties of the Ir catalyst measured by BET adsorption method, hydrogen adsorption measurement and X-ray photoelectron spectroscopy.

Sample	5 wt% Ir/Al_2O_3	10 wt% Ir/Al_2O_3	20 wt% Ir/Al_2O_3
Loading (wt%)[a]	5.8	9.8	16.4
BET surface area ($m^2\ g^{-1}$)	112	129	130
Pore volume ($cm^3\ g^{-1}$)	0.33	0.35	0.31
H adsorption ($\mu mol\ g^{-1}$)	227	390	557
Dispersion (%)[b]	75	77	65
Particle size (nm)[c]	1.3	1.3	1.5

[a] Elemental analysis by X-ray photoelectron spectroscopy.
[b] Assuming the adsorption stoichiometry is one hydrogen per Pt atom.
[c] Assuming spherical particle, d (nm) = 100/dispersion (%).

Surface properties of the Ir catalyst are listed in Table 1. The metal loading measured from XPS was similar to that of the nominal loading up to 10 wt%. Further increase of metal loading to 20 wt% gave underestimated metal loading 16.4 wt%. The BET surface area increased slightly with the metal content with the slight variation of the pore volume due to the increase of surface area of metal catalyst, or the number of metal particles. Measurement of hydrogen adsorption on Ir catalyst gave an interesting result corresponding to ~70% dispersion. Such high dispersion indicated the formation of 1.3–1.5 nm particle much smaller than the size of Ir nanoparticle with higher loading such as 30 wt% assuming spherical particle geometry [12]. It was of note that the 16.4 wt% Ir catalyst showed 557 $\mu mol\ g^{-1}$. This high hydrogen adsorption was comparable to that of the 30 wt% Ir catalyst, 600–650 $\mu mol\ g^{-1}$. Therefore, it seemed that the decreasing metal content to a half did not cause a significant reduction of hydrogen adsorption which is necessary for the catalytic decomposition of NH_3 and N_2H_4.

High resolution transmission electron micrographs of the Ir catalyst are shown in Fig. 3. The number density of the Ir nanoparticle was increased with the increase of the metal content. The particle size was in the range of 1–2 nm and the lateral spacing between the particles was less than 10 nm. The metal particle was distributed evenly over the entire catalyst surface. Highly magnified micrograph of the Ir nanoparticle shows the 7–8 atomic layers in the particle, which meant the formation of 1.8 nm sized particle. The particle shape seemed to be raft-like at low loading and became spherical with the increase of the metal content.

It should be noted that the separation between the iridium particles was almost the same as the dimensions of the particle size. Iridium particles might be susceptible to agglomeration due to the small separation. However, the agglomeration of the iridium particles was suppressed under a hydrogen atmosphere possibly due to the strong metal–support interaction.

Such textural properties of the Ir catalyst were also reflected in the AFM image presented in Fig. 4. At 5.9 wt% loading, the very rough surface was obtained, partly consistent with the formation of 1–2 nm sized nanoparticles. Increasing the metal content, the texture of the surface became smooth probably due to that the number density of the particle over the catalyst surface was so high that the AFM tip can detect only the Ir metal. A series of the AFM image as a function metal content suggested that the catalyst surface was covered fully with the Ir nanoparticles and it became smooth.

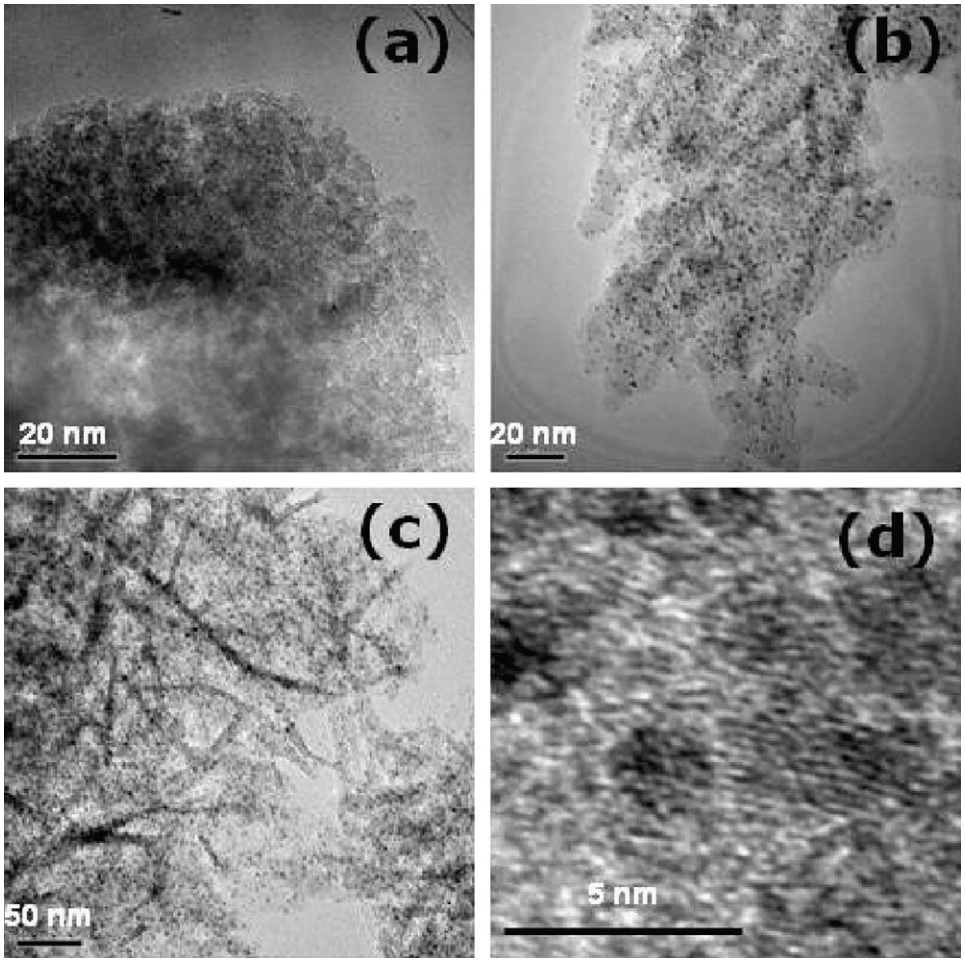

Fig. 3. HRTEM micrographs of (a) 5 wt% Ir/Al_2O_3, (b) 10 wt% Ir/Al_2O_3 and (c and d) 20 wt% Ir/Al_2O_3.

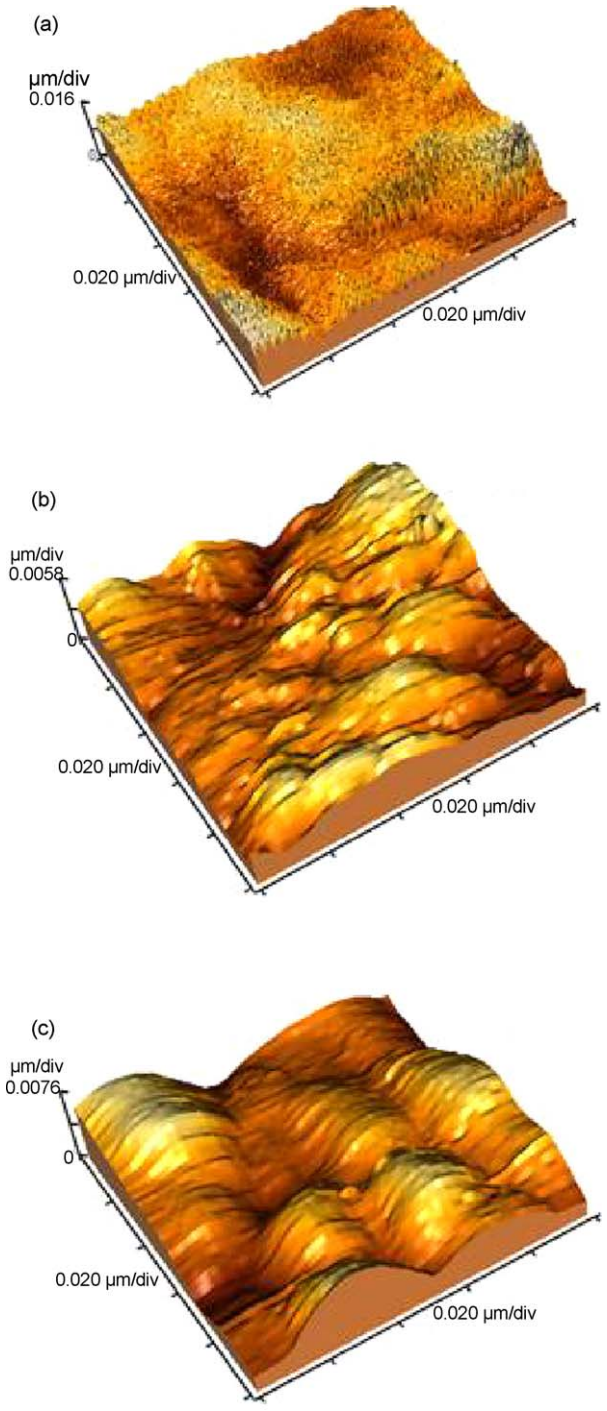

Fig. 4. Surface of the catalyst of (a) 5 wt% Ir/Al_2O_3, (b) 10 wt% Ir/Al_2O_3 and (c) 20 wt% Ir/Al_2O_3 probed with AFM.

Fig. 5 shows the EXAFS spectrum and its corresponding k^3-weighted Fourier transform of the Ir catalyst as a function of Ir content. The XAFS data was analyzed using the UWXAFS2 program [13,14]. The background of raw X-ray absorption data was removed using the method proposed by Newville at al. [14] in which the low *R*-component in Fourier transform of XAFS spectrum was minimized comparing with either theoretical standard from *Feff* code [10] or experimental standard contained a correct background. After the removal of background, XAFS oscillations were normalized using edge jump and was weighted by k^3 as shown in Fig. 5. $k^3\chi(k)$ in the range of 30–130 nm^{-1} was

Table 2
Structural parameters obtained from EXAFS curve fitting for the Ir catalyst.

Sample	Pair	N[a]	R (nm)[b]	(^{2} (pm^2)[c]	(E (eV)[d]	R-factor[e]
5 wt% Ir/Al_2O_3	Ir–O	2.9	0.202	72	16.2	0.059
	Ir–Al	1.1	0.245	46		
	Ir–Ir	1.6	0.267	53		
10 wt% Ir/Al_2O_3	Ir–O	2.9	0.202	77	18.8	0.018
	Ir–Al	1.0	0.251	37		
	Ir–Ir	3.5	0.268	65		
20 wt% Ir/Al_2O_3	Ir–O	2.1	0.196	71	9.9	0.045
	Ir–Ir	7.7	0.269	80		

Number of independent free parameters, N_{idp} and variable, N_{var} in the fit were 10 and 6, respectively, which was given by $N_{idp} = (2\Delta k \cdot \Delta r/\pi) + 2$ where Δk and Δr were 100 nm^{-1} (30–130 nm^{-1}) and 0.159 nm (0.149–0.308 nm, respectively).
[a] Coordination number (±0.5).
[b] Bond distance (±0.001 nm).
[c] The Debye–Waller factor.
[d] E_0 shift used in the fit.
[e] *R*-factor to measure the quality of the fit.

Fourier transformed into *R*-space for the curve fit. The curve fitting routine, FEFFIT, can use theoretical *Feff* standards when it was very difficult to get experimental XAFS spectrum for standard of which the crystal structure is known accurately. The obtained structural parameters are listed in Table 2. Three atomic pair distribution functions for low loading Ir catalyst were obtained, an Ir–Ir pair at 0.27 nm, an Ir–Al pair at 0.25 nm and an Ir–O pair at 0.20 nm. The

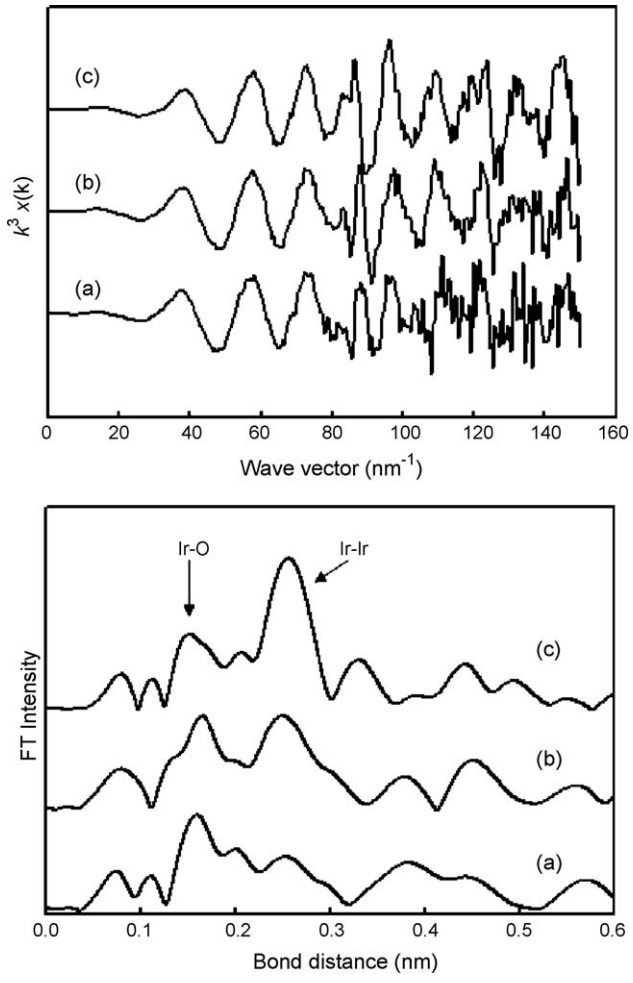

Fig. 5. k^3-weighted EXAFS spectra and the corresponding Fourier transform of the catalysts: (a) 5 wt% Ir/Al_2O_3, (b) 10 wt% Ir/Al_2O_3 and (c) 20 wt% Ir/Al_2O_3.

Table 3
Binding energy of the Ir catalyst measured by X-ray photoelectron spectroscopy.

Sample	Binding energy (eV)[a]		
	Al 2p	Ir $4f_{5/2}$	Ir $4f_{7/2}$
5 wt% Ir catalyst	74.70	64.84	61.76
10 wt% Ir catalyst	74.54	65.07	61.92
20 wt% Ir catalyst	74.51	64.87	61.81

[a] Referenced to the binding energy of the O 1s in Al_2O_3.

detection of the Ir–Al pair distribution indicated the strong metal–support interaction. The Ir–Al pair distribution became disappeared with the increase of the metal content systematically again. The Ir–Ir pair distribution increased from 1.6 to 7.7 with the increase of the metal content, which consistent with the particle shape and the textural properties obtained from the TEM observation and the AFM measurement. Further the structure contained the Ir–Ir distance, which is different from those in IrO_2, 0.315 nm and 0.355 nm. Rather, it was very similar to that of Ir metal, indicating an Ir metal structure surrounded by oxygen.

The Ir–O distribution was decreased slightly from 2.9 to 2.1. Such small Ir–O coordination suggested the presence of the adsorbed oxygen. From the coordination number, it seemed that the structure of Ir nanoparticle was the Ir metal core covered with oxygen.

Electronic structure of the Ir nanoparticle was probed with X-ray photoelectron spectroscopy. Fig. 6 and Table 3 show the XPS spectra of the Ir binding energy in the catalyst. The binding energy of Ir $4f_{5/2}$ and Ir $4f_{7/2}$ was shifted to higher energy referenced to that of the O 1s in Al_2O_3. This was consistent with the partially oxidized Ir nanoparticle since the reduced Ir metal core was covered with the adsorbed oxygen. Therefore, the results from XPS were consistent with the results of TEM, AFM and EXAFS.

Fig. 7 shows the hydrazine hydrate decomposition on the honeycomb catalyst at room temperature. The pulse injection was performed in 20 cycles consisting of 100 ms on time and 5 s cycle time that was equal to 0.2 ml injection. The injection pressure was 85 psi. Before the start-up, nitrogen gas was purged for 10 min with

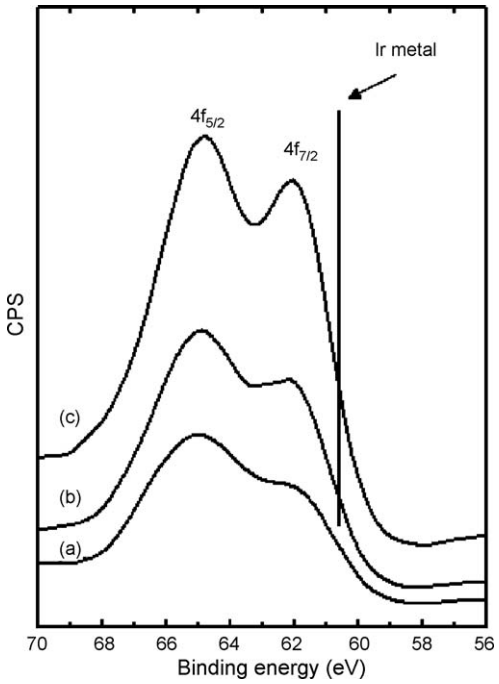

Fig. 6. XPS spectra of the Ir catalysts: (a) 5 wt% Ir/Al_2O_3, (b) 10 wt% Ir/Al_2O_3 and (c) 20 wt% Ir/Al_2O_3.

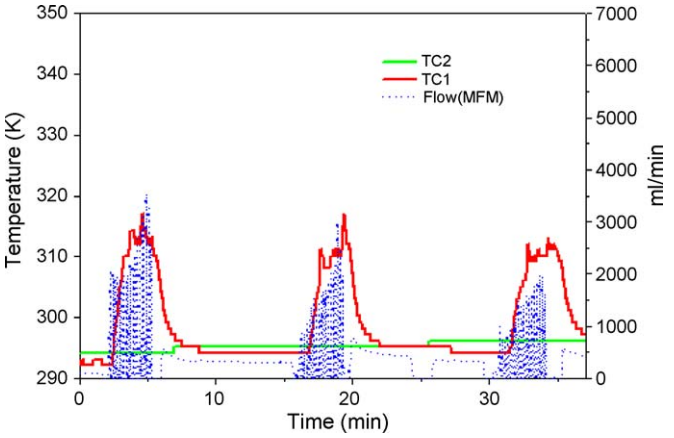

Fig. 7. Hydrazine decomposition reaction on the honeycomb catalyst at room temperature. The gas evolution was monitored in differential mode. The pulse injection was performed in 20 cycles consisting of 100 ms on time and 5 s cycle time.

of flow rate of 100 ml min^{-1}. Also, the nitrogen was injected continuously between the reactions to remove the product gas. From the blank honeycomb testing, there was no gas evolution at all and also no temperature rise upon hydrazine hydrate injection. While, the decomposition reaction was proceeded readily even at room temperature when the honeycomb catalyst containing Ir was installed. The temperature rise at TC1 where liquid droplet of micronsize, e.g. 9 μm, was sprayed on the catalyst initially was ca. 30–40 K. The gas evolution was decreased when the cycle was repeated. Such a decrease was attributed to the decrease of catalytic activity. However, the catalytic activity or the gas evolution was recovered when the catalyst was heated at 573 K under nitrogen flow to remove the residual product water since the hydrazine hydrate contained a lot of water, 44.9 wt%.

Therefore, the reaction temperature at TC3 was increased to 423 K to remove the water. Also, the water removal unit was installed after TC2 as shown in Fig. 1. The temperature at TC2 was thus 393 K enough to remove the water though the temperature at TC1 was fluctuated upon the hydrazine hydrate injection similar to that in Fig. 7. The hydrazine hydrate decomposition was occurred without the deterioration of catalyst activity as shown in Fig. 8. The gas evolution was proportional to the number of cycle and maintained to be the same for the cycle measurement. The temperature rise and fall at TC1 was the same for all cycle as illustrated. Initially, the concentration of NH_3 in effluent gas was ca.

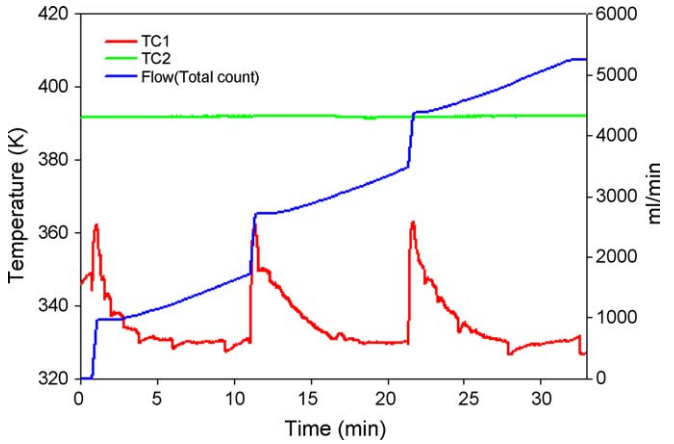

Fig. 8. Hydrazine decomposition reaction on the honeycomb catalyst at 473 K in 20 cycles-pulse mode where the on and cycle time were 100 ms and 1 s, respectively. The gas evolution was monitored in integral mode. The temperature of TC3 was maintained at 473 K to remove the water.

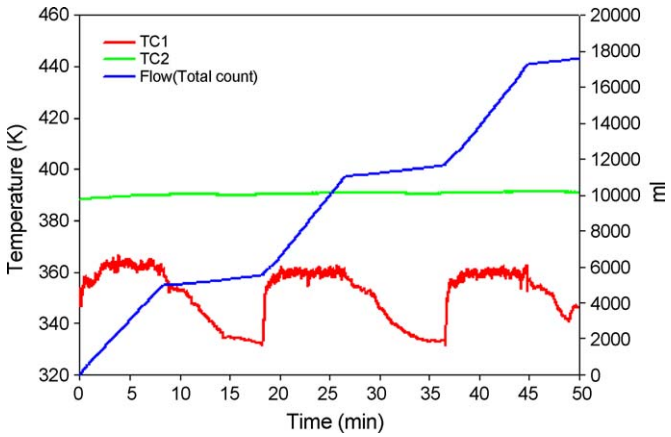

Fig. 9. Continuous pulse mode hydrazine decomposition reaction on the honeycomb catalyst at 473 K.

600 ppm and decreased to near zero level, suggesting that there was no appreciable formation of NH_3 or the dissolution of NH_3 into water. Therefore, the evolved gas did not contained NH_3 at all.

Fig. 9 shows the result of the continuous pulse mode reaction. The reaction was proceeded readily without significant deterioration of the catalyst activity. The gas evolution was proportional to the number of pulse. Such a continuous reaction can be occurred more than several hours if the residual water is removed properly since the hydrazine hydrate contained a lot of water, 44.9 wt% as indicated above.

4. Conclusion

The structure of Ir catalyst containing 5–16 wt% metal content was characterized with AFM, HR-TEM, EXAFS, etc. The obtained raft-like particle shape became the spherical one with the increase of metal content. Using the present iridium containing honeycomb catalyst, the study on the catalytic activity over hydrazine hydrate decomposition showed that the reaction can occur readily near ambient temperature if the residual water is removed properly with the elevation of reaction temperature above 373 K and the use of water trap. More detailed study on the reaction characteristics is in progress.

Acknowledgment

This work was supported by the Hydrogen Energy R&D Center, one of the 21st Century Frontier R&D Programs, funded by the Ministry of Science and Technology, Korea.

References

[1] E.W. Schmidt, Hydrazine and its Derivatives: Preparation, Properties, Applications, Wiley-Interscience, New York, 1984.
[2] W.E. Armstrong, L.B. Ryland, H.H. Voge, US Patent 4,124,538 (1978).
[3] G. Papapolymerou, V. Bontozoglou, J. Mol. Catal. A 120 (1997) 165.
[4] S.J. Cho, J. Lee, Y.S. Lee, D.P. Kim, Catal. Lett. 3–4 (2006) 181.
[5] A.M. Argo, B.C. Gates, Langmuir 18 (2002) 2152.
[6] F. Li, B.C. Gates, J. Phys. Chem. B 108 (2004) 11259.
[7] A.M. Argo, J.F. Odzak, B.C. Gates, J. Am. Chem. Soc. 125 (2003) 7109.
[8] C. Pak, S.J. Cho, J.Y. Lee, R. Ryoo, J. Catal. 149 (1994) 61.
[9] (a) S.J. Cho, W.S. Ahn, S.B. Hong, R. Ryoo, J. Phys. Chem. 100 (1996) 4996; (b) R. Ryoo, S.J. Cho, C. Pak, J.Y. Lee, Catal. Lett. 20 (1993) 107.
[10] J.J. Rehr, R.C. Albers, S.I. Zabinsky, Phys. Rev. Lett. 69 (1992) 3397.
[11] (a) P. Scherrer, Nachr. Ges. Wiss. Gottigen, Math-Phys. K1 2 (1918) 96; (b) R. Jenkins, R.L. Synder, Introduction to X-ray Powder Diffractometry, John Wiley & Sons, New York, 1996.
[12] M. Boudart, G. Djega-Mariadassou, Kinetics of Heterogeneous Catalytic Reactions, Princeton University Press, Princeton, NJ, 1984.
[13] E.A. Stern, M. Newville, B. Ravel, Y. Yacoby, D. Haskel, Physica B 208 (1995) 117.
[14] M. Newville, P. Livins, Y. Yacoby, J.J. Rehr, E.A. Stern, Phys. Rev. B 47 (1993) 14126.